Desalination and Water Treatment
www.deswater.com
doi: 10.5004/dwt.2021.27232

226 (2021) 125–136
June

Decomposition of nitrobenzene in wastewater using persulfate combined with Ag/PbO under ultrasonic irradiation

Wen-Shing Chen*, Tang-Yao Chang

Department of Chemical and Materials Engineering, National Yunlin University of Science and Technology, 123 University Road, Section 3, Douliou, Yunlin 640, Taiwan, Tel. +886-5-534-2601, Ext: 4624; Fax: 886-5-531-2071; emails: chenwen@yuntech.edu.tw (W.-S. Chen), m10815005@yuntech.edu.tw (T.-Y. Chang)

Received 19 November 2020; Accepted 11 March 2021

ABSTRACT

Nitrobenzene oxidation was executed by means of a novel process, wherein persulfate anions were combined with Ag/PbO semiconductors activated by ultrasound. Batch-wise experiments were accomplished to investigate the influence of ultrasonic power intensity, persulfate concentrations, and Ag/PbO dosages, respectively, on the nitrobenzene removal efficiency. Owing to pronounced scavenging effects exhibited by benzene, ethanol, and methanol individually, the principal oxidizing agent was sensibly presumed to be sulfate radicals, which could be generated from persulfate anions activated with sonocatalysis of Ag/PbO. The optimal conditions for complete elimination of nitrobenzene were found as follows: ultrasonic power intensity = 240 W cm^{-2}, T = 318 K, persulfate concentration = 70 mM, and Ag/PbO dosage = 1.3 g L^{-1}. As far as oxidation pathways are concerned, nitrobenzene was initially transformed into hydroxycyclohexadienyl radicals, followed by the formation of 2-nitrophenol or 4-nitrophenol. Denitration of nitrophenol compounds makes the synthesis of phenol, which was sequentially converted into hydroquinone and *p*-benzoquinone.

Keywords: Nitrobenzene; Persulfate; Ag/PbO semiconductor; Sulfate radical

1. Introduction

Nitrobenzene is an extremely important petrochemical for the production of polyurethane through the reaction pathway of aniline. Its derivatives have been also applied for the manufacturing dyes, explosives, pesticides, and pharmaceutical industry [1]. Nonetheless, the wastewater contaminated with nitrobenzene and related derivatives would cause a serious impact on the environment due to its inherent mutagenicity and plausible carcinogenicity [2,3]. The industrial effluent disposal was always an objective to be investigated.

Owing to the electron-withdrawing effect of the nitro group on the biodegradation inhibition, advanced oxidation processes have been extensively developed for the decomposition of nitrobenzene in wastewater [4]. With regard to methods for titanium dioxide, the nitrobenzene removal rate by photocatalysis could be significantly accelerated over TiO_2 impregnated with Fe_2O_3 or Li_2O, which effectively retards recombination of photogenerated holes and electrons, resulting in enhancement of hydroxyl radical numbers [5]. Besides, the absorption band of TiO_2 could be broadly shifted to the visible light range using a sol–gel manner with impregnation of ammonium nitrate and cerium nitrate [6,7]. On the other hand, hydroxyl radicals derived from ozone under ultrasonic irradiation were used for the mineralization of nitrobenzene. The cavitation strength seems to be a crucial factor [8,9]. Ozone integrated heterogeneously with honeycomb (Al_2O_3–SiO_2) [10–14] or ZSM-5 [15] has been wildly employed for disposal of

* Corresponding author.

wastewater contained nitrobenzene. The electrochemical processes also showed effective oxidation ability for nitrobenzene by means of incorporation of TiO_2 nanotubes into PbO_2 electrode plates, leading to high specific surface areas and ordered orientation [16–18]. Moreover, hydroxyl radical-based Fenton processes have been explored, including homogeneous Fenton's reagents [19,20], heterogeneous Fenton reagents [21], Fenton-like reagents [22–25], Fenton/ultrasound [26], and fluidized-bed Fenton process [27,28].

Recently, oxidative degradation of nitrobenzene in wastewater via sulfate radical-based processes has achieved much interest. Heat-activated persulfate technique was applied for decomposition of nitrobenzene, of which reaction intermediates include 2-nitrophenol, 4-nitrophenol, 2,4-dinitrophenol, and 2,6-dinitrophenol [29]. Besides, persulfate integrated with either Fe(II)/UV or O_3 was verified to be an efficient method on account of the significant generation of sulfate radicals [30,31]. Persulfate anions could be successfully activated via either zero-valent Zn^0/ultrasound [32] or magnetized Fe^0 [33,34]. As regards acoustic processes, the cavitation phenomenon would come into occurrence with steady emission of sonoluminescence simultaneously, of which wavelength was believed to fall in the region of 200–700 nm [35,36]. The luminous energy of sonoluminescence, in coincidence with the bandgap energy of some semiconductors, could stimulate them to generate electron–hole pairs. Persulfate anions may be transformed into sulfate radicals via activation with previous sono-induced electrons [37].

In this work, a novel process for the elimination of nitrobenzene in wastewater would be established. Persulfate anions could be greatly converted into sulfate radicals upon activation with both ultrasound and sonocatalysis of Ag/PbO, recognized as semiconductors [38–41]. The influential factors on the nitrobenzene removal performance were investigated, including ultrasonic power intensity, persulfate concentrations, and Ag/PbO dosages. Additionally, nitrobenzene oxidation pathways by the persulfate integrated with Ag/PbO under ultrasonic irradiation were also presented.

2. Experimental methods

2.1. Testing of persulfate coupled with Ag/PbO under ultrasonic irradiation

Fig. 1 depicts the schematic illustration of the overall experimental apparatus. The ultrasonic irradiation was supplied at the frequency of 20 kHz with adjustable power intensity (Chrom Technol. Corp., USA, UP-800 Model), wherein a titanium probe (F13 mm × 60 mm) was partially immersed into the aqueous solution. The double jacket cylinder served as the sonocatalytic reactor, in which Ag/PbO was packed into a basket (PIIN JIA Technol. Corp., JC-A16 Model). The temperature of wastewater was maintained at 318 ± 0.5 K by a thermostat referred to our previous work [42]. According to real situation of industrial wastewater, the synthesized feedstock, composed of 1.0 mM concentrations of nitrobenzene (≥99.9%, Riedel-de Haen) [43], was well-agitated with proportional weight of sodium persulfate (≥99.5%, Fluka). The Ag/PbO,

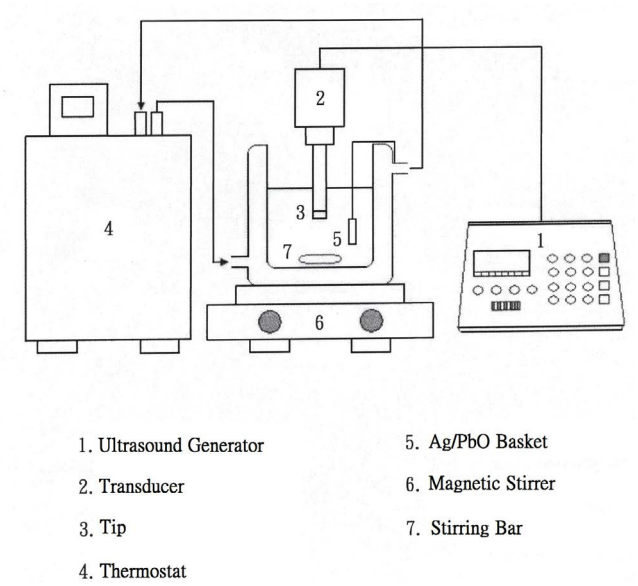

Fig. 1. Scheme of the experimental apparatus employed by persulfate integrated with Ag/PbO under ultrasonic irradiation.

synthesized from PbO powder impregnated by incipient wetness with various concentrations of silver nitrate (≥99.5%, Riedel-de Haen) and sequentially calcined at 823 K for 3 h and sieved over 400 mesh [44], was located into the basket. Within the course of tests, wastewater was sampled from the reactor at the same time interval, immediately cooled to temperature of 273 ± 0.5 K to quench oxidation reaction [45]. Total organic carbon (TOC) analyses were carried out on the samples to evaluate the organic compound content. The Ag/PbO retrieved after oxidation tests would execute X-ray photoelectron spectroscopy (XPS).

In this research, experiments were performed batch-wisely under a series of ultrasonic power intensities of 120, 180, 240, and 300 W cm^{-2} (as quoted by the manufacturer). Additionally, four tests with changeable persulfate anion concentrations (50.0–80.0 mM) were carried out. The sonocatalytic tests were also undertaken with diverse Ag/PbO dosages (0.7 up to 1.6 g L^{-1}) for enhancement of nitrobenzene removal rate. Experiments were conducted under various initial pH values (3.0–7.0) to elucidate the oxidants for nitrobenzene oxidation, wherein the acidity of wastewater was adjusted through the addition of appropriate amounts of sulfuric acid solution (0.1 M). On the other hand, the adsorption testing was undergone to disclose the physical adsorbability of nitrobenzene on the Ag/PbO. The conical flasks, containing wastewater (300 mL) at 1.0 mM nitrobenzene and designed amounts of Ag/PbO, were situated in the shaker (Deng Yng Corp., DKW-50L Model, Taiwan) with a vibration speed of 120 rpm for 6 h. The residual nitrobenzene in wastewater would be determined using a TOC instrument. In this study, all experiments were performed to the least extent for validation of data.

2.2. Total organic carbon analysis

Within the period of tests for persulfate integrated with Ag/PbO under ultrasonic irradiation, wastewater

was regularly withdrawn and directly undergone analyses using a TOC instrument (GE Corp., USA, Sievers InnovOx). The hydrocarbons involved would be quantified by a non-dispersive infrared (NDIR) instrument through carbon dioxide generated from persulfate oxidation with the assistance of supercritical water conditions. Conversely, the non-hydrocarbon was transformed into carbonic acid. TOC concentrations reported were based on the calibration curve, established precisely among the range (0–4.0 mM) utilizing potassium hydrogen phthalate standard solutions.

2.3. Physicochemical properties of Ag/PbO

For a series of Ag/PbO semiconductors, the ultraviolet-visible diffuse reflectance spectra (DRS) were procured by means of an UV-vis spectrometer (PerkinElmer Corp., USA, Lambda 850 Model). The UV-DRS obtained were among the wavelength range of 380–800 nm based on the reference of $BaSO_4$. According to scanning from a field-emission scanning electron microscopy (FE-SEM, JSM-6500F, JEOL) equipped with energy-dispersive X-ray spectroscopy (EDS, JED-2300, JEOL), Ag/PbO semiconductors were examined for their surface morphology and weight content of silver-impregnated. Besides, XPS profiles, given by the X-ray photoelectron spectrometer coupled with the monochromatic AlKα source (Kratos Analytical Ltd., UK, Axis Ultra), were used to elucidate electronic states on original and reacted Ag/PbO semiconductors. The C 1s core level at 284.8 eV for adventitious carbon served as standard binding energy.

2.4. Gas chromatography-mass spectrometry analysis

After 3 h operation testing for persulfate coupled with Ag/PbO under ultrasonic irradiation, the amount of 300 mL wastewater was withdrawn from the sonocatalytic reactor. The sample was mixed with microextraction fiber made of Carboxen/Polydimethylsiloxane (Supelco., USA), to adsorb oxidative degradation intermediates. Then, the fiber was retracted into a protective needle and sequentially inserted into an injection port of gas chromatography-mass spectrometer (Hewlett Packard 59864B/HP 5973 MASS, USA). Helium gas served as carrier gas and an analytic capillary column was used with dimensions of 30 m × 0.25 mm (Metal ULTRA ALLOY UA-5). According to the mass spectra obtained with reference to those of standards, the majority of degradation intermediates of nitrobenzene were confidently determined.

2.5. Scavenging effects

By means of the addition of various scavengers, such as benzene, ethanol, and methanol, respectively, mineralization of nitrobenzene using persulfate integrated with Ag/PbO under ultrasonic irradiation was carried out for elucidation of chief oxidizing agents [46,47]. The nitrobenzene removal percentage was directly examined through the peak at 262 nm shown on a UV-vis spectrophotometer (PerkinElmer Inc., USA, Lambda 850) [21]. For comparison of sulfate radical yields under different operating conditions, appropriate amounts of benzene scavenger were added to wastewater accompanied with nitrobenzene simultaneously to present the decrement of nitrobenzene removal percentage. Thus, the benzene scavenging index may substitute for sulfate radical yields in this study.

3. Results and discussion

3.1. Comparison of persulfate oxidation and persulfate coupled with Ag/PbO under ultrasonic irradiation

Fig. 2a presents the time-dependent patterns of TOC removal percentage executed by persulfate oxidation and persulfate coupled with Ag/PbO, respectively, activated with ultrasound. Apparently, the nitrobenzene removal percentage caused by persulfate integrated with Ag/PbO process was much higher than those using persulfate oxidation alone and persulfate integrated with PbO process. This phenomenon may be interpreted with enhancement on sulfate radical yields. It has been acknowledged that persulfate anions activated by ultrasound [42] or sonocatalysis of Ag/PbO semiconductors [48,49] could be converted into sulfate radicals. Additionally, Ag metal was admitted to function as an electron sink and reinforced charge separation, leading to inhibition of recombination of sonogenerated electrons with holes on the surface of PbO and promotion of persulfate activation [50,51]. The reactions inferred are shown as follows:

$$S_2O_8^{2-} +))) \rightarrow 2SO_4^{\bullet -} \quad (1)$$

$$Ag/PbO +))) \rightarrow h_{vb}^{+} + e_{cb}^{-} \quad (2)$$

$$S_2O_8^{2-} + e_{cb}^{-} \rightarrow SO_4^{\bullet -} + SO_4^{2-} \quad (3)$$

$$SO_4^{2-} + h_{vb}^{+} \rightarrow SO_4^{\bullet -} \quad (4)$$

wherein e_{cb}^{-} stands for sonogenerated electrons in the conduction band and h_{vb}^{+} stands for sonogenerated holes in the valence band.

The adsorption tests for Ag/PbO semiconductors were performed in the dark in order to make clear the nitrobenzene removal routes. The results clearly indicate that nitrobenzene adsorbed physically over the Ag/PbO was present in trace (Fig. 2b). Obviously, nitrobenzene is expected to be abated via an oxidation pathway.

3.2. Physicochemical and optical properties of Ag/PbO

The FE-SEM images of Ag/PbO semiconductors are demonstrated in Fig. 3. As shown in Fig. 3a, the most surface of PbO was smooth. Nonetheless, for consideration of PbO doped with Ag metal, some irregularly shaped particles in clumps deposited on PbO were observed (refer to Figs. 3b–f). As the amount of Ag loaded was increased, more clumps of particles existed. It points out that Ag was well-dispersed on the surface of PbO. The EDS element analyses on Ag/PbO semiconductors are listed in Table 1. It shows that the weight percentage of Ag measured on the surface of PbO was consistent with that impregnated theoretically.

Fig. 4 illustrates the UV-vis DRS of Ag/PbO semiconductors. The spectrum of PbO exhibits strong absorbance between the wavelength of 430 and 610 nm, which belongs

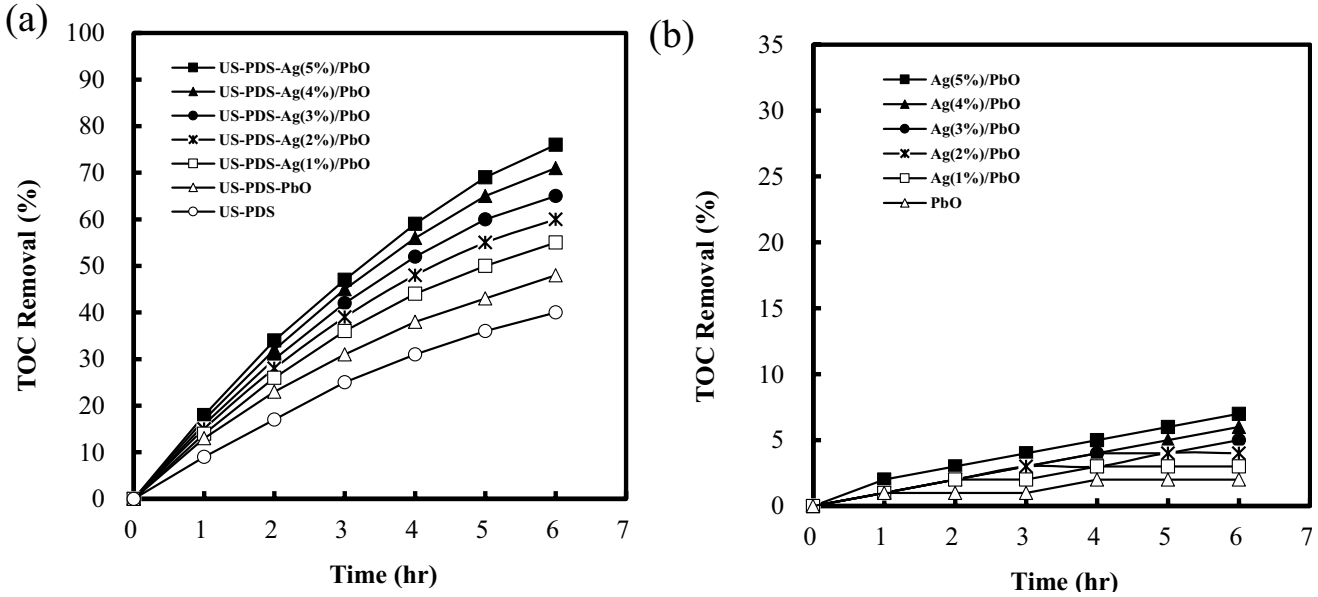

Fig. 2. (a) Time-dependent patterns of TOC removal percentage by PbO, Ag(1 wt.%)/PbO, Ag(2 wt.%)/PbO, Ag(3 wt.%)/PbO, Ag(4 wt.%)/PbO and Ag(5 wt.%)/PbO, respectively, under the conditions of ultrasonic power intensity = 240 W cm^{-2}, T = 318 K, persulfate concentration = 60 mM and Ag/PbO dosage = 1.0 g L^{-1}. (b) Time-dependent patterns of TOC removal percentage by means of adsorption on the surface of PbO, Ag(1 wt.%)/PbO, Ag(2 wt.%)/PbO, Ag(3 wt.%)/PbO, Ag(4 wt.%)/PbO and Ag(5 wt.%)/PbO, respectively, in the dark under the conditions of T = 318 K, PbO dosage = 1.0 g/L or Ag/PbO dosage = 1.0 g/L.

to the visible light region. Especially, the spectra of Ag/PbO present a sharp absorbance peak near the wavelength of 420 nm and a broader absorbance between the wavelength of 450 and 650 nm. It appears that Ag/PbO semiconductors are more responsive to visible light irradiation than PbO. The observation may be ascribed to Ag metal dopant, supplying an electron pool and preventing recombination of photogenerated electrons with holes on the surface of PbO [52,53]. Furthermore, the bandgap energy of Ag/PbO was estimated in accordance with Tauc's equation [$(\alpha h\nu)^{1/n} = A(h\nu - E_g)$], in which hν means incident energy. The "n" value was commonly set as the value of 1/2 or 2 based on the electronic transition state of semiconductors. The variation of $(\alpha h\nu)^2$ vs. incident energy (hν) was drawn to evaluate the bandgap energy, obtained by intercepting the tangent to the X-axis [54–56]. Thus, the bandgap energy of PbO was estimated to be 1.99 eV, consistent with the publication by Droessler et al. [57]. The bandgap energy of a series of Ag/PbO semiconductors was determined between 1.60 and 1.83 eV, lower than that of PbO (Table 2). It is worthy that Ag/PbO was beneficial to activate persulfate for oxidation of nitrobenzene under ultrasound (Fig. 2a). The superior sonocatalytic behavior over Ag(5%)/PbO may be attributed to much enhancement on charge conduction and lower bandgap energy, more sensitivity to visible light, and sonoluminescence. Owing to the higher degradation efficiency of nitrobenzene, Ag(5%)/PbO was chosen as a candidate for further tests. In this study, the energy of sonoluminescence, certainly greater than the bandgap energy of the Ag/PbO semiconductors, could excite them to generate electron–hole pairs. The sonogenerated electrons in the conduction band may activate persulfate anions into sulfate radicals, whereas sonogenerated holes in the valence band may also convert sulfate anions into sulfate radicals (Eqs. (3) and (4)).

XPS measurements were performed for clarification of intrinsic electronic state of Ag(5%)/PbO. Fig. 5 presents the Pb 4f XPS spectra of original Ag(5%)/PbO and Ag(5%)/PbO reacted. With regard to original Ag(5%)/PbO semiconductor, two peaks centered at 138.7 and 143.7 eV were observed, which were assigned to the binding energy of Pb $4f_{(7/2)}$ and Pb $4f_{(5/2)}$, respectively [58–60]. Nevertheless, the binding energy of Pb $4f_{(7/2)}$ and Pb $4f_{(5/2)}$ of Ag(5%)/PbO has shifted to 139.9 and 144.8 eV individually after nitrobenzene oxidation testing. It clearly indicates that Pb cations on the surface of Ag(5%)/PbO make a deviation to higher oxidation states in comparison with the original one, due to migration of sonogenerated electrons to persulfate anions [61,62]. The outcomes approve the above hypothesis that persulfate anions could be activated by sonogenerated electrons into sulfate radicals. Besides, Ag(5%)/PbO may adsorb sulfate anions [63], which were sequentially transformed into sulfate radicals by means of sonogenerated holes. It would make partial contributions to degradation of nitrobenzene.

3.3. Effect of dosage of scavengers on persulfate coupled with Ag/PbO under ultrasonic irradiation

Equivalent concentrations of benzene, ethanol, and methanol, respectively, accompanied with nitrobenzene were blended in wastewater to clarify reactive radicals for persulfate integrated with Ag/PbO activated by ultrasound. As illustrated in Fig. 6, the nitrobenzene removal percentage was obviously declined upon the addition of benzene. The rate constant between benzene and sulfate

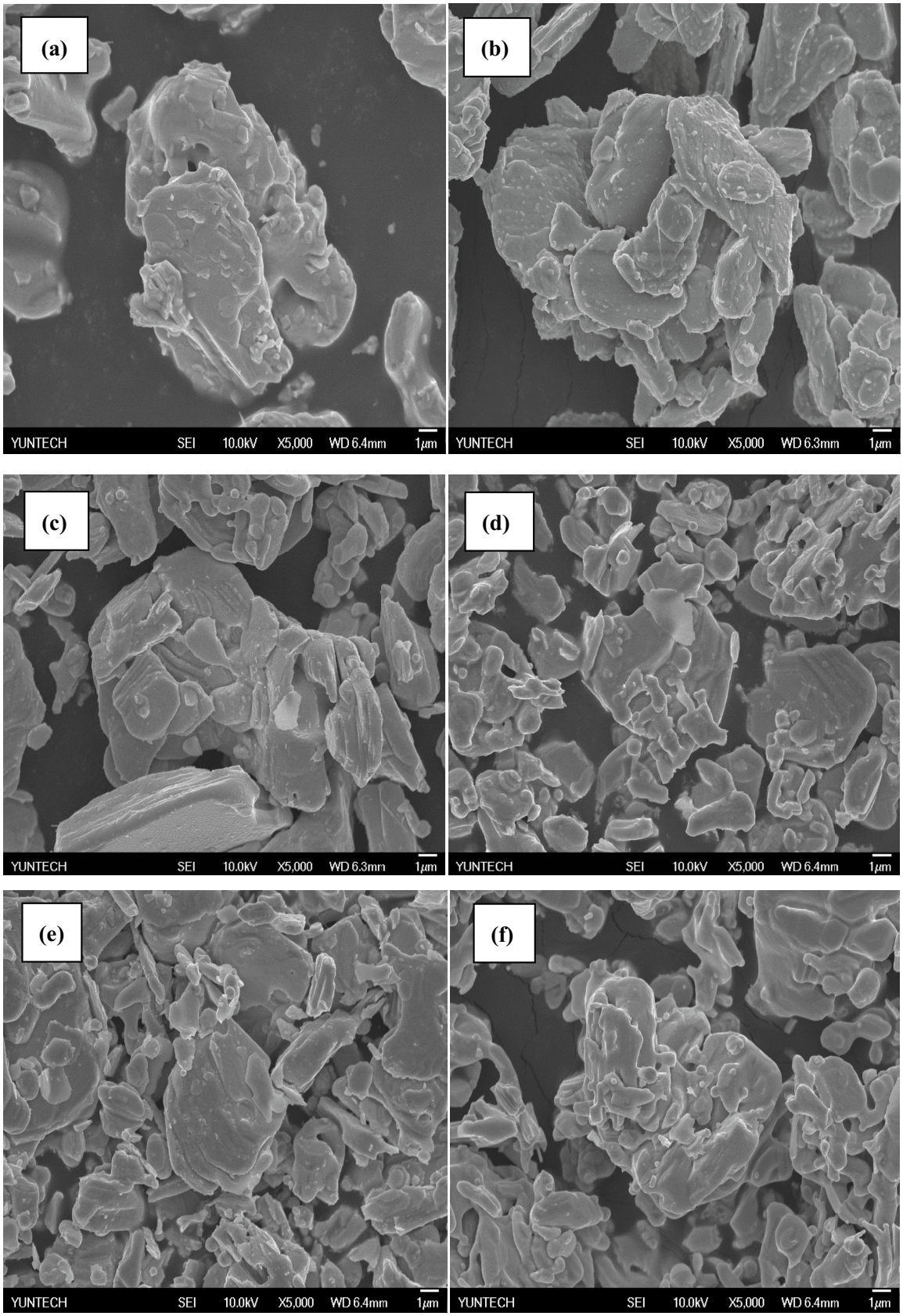

Fig. 3. FE-SEM images of the (a) PbO, (b) Ag(1 wt.%)/PbO, (c) Ag(2 wt.%)/PbO, (d) Ag(3 wt.%)/PbO, (e) Ag(4 wt.%)/PbO and (f) Ag(5 wt.%)/PbO semiconductors.

Table 1
EDS element analyses on Ag/PbO semiconductors

Semiconductor	Pb (wt.%)	O (wt.%)	Ag (wt.%)
PbO	56.6	43.4	0
Ag(1 wt.%)/PbO	55.31	43.85	0.84
Ag(2 wt.%)/PbO	55.35	42.82	1.83
Ag(3 wt.%)/PbO	51.49	45.47	3.04
Ag(4 wt.%)/PbO	52.15	44.06	3.79
Ag(5 wt.%)/PbO	54.67	40.44	4.89

Table 2
Band-gap energy of Ag/PbO semiconductors determined by UV-DRS

Semiconductors	Band-gap energy (eV)
PbO	1.99
Ag(1 wt.%)/PbO	1.83
Ag(2 wt.%)/PbO	1.79
Ag(3 wt.%)/PbO	1.70
Ag(4 wt.%)/PbO	1.65
Ag(5 wt.%)/PbO	1.60

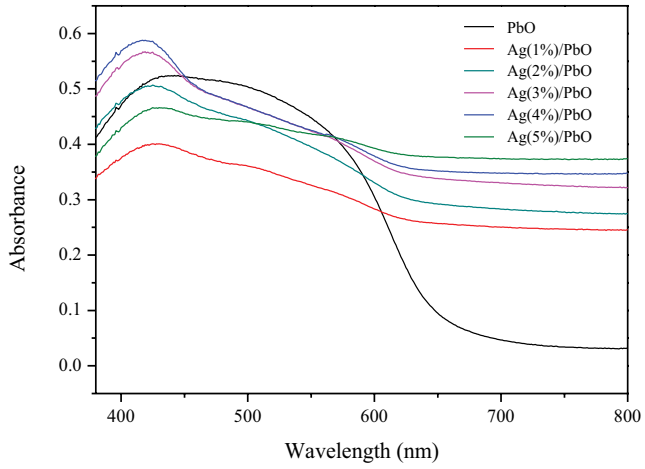

Fig. 4. UV-vis diffuse reflectance spectra of PbO, Ag(1 wt.%)/PbO, Ag(2 wt.%)/PbO, Ag(3 wt.%)/PbO, Ag(4 wt.%)/PbO and Ag(5 wt.%)/PbO semiconductors.

radicals has been reported to be 3 × 10^9 M^{-1} s^{-1} [46]. In another aspect, ethanol and methanol input inhibited the abatement of nitrobenzene moderately. Ethanol and methanol reacted with sulfate radicals at the rate constants of 7.7 × 10^7 and 3.2 × 10^6 M^{-1} s^{-1}, separately [64]. Transparently, the decay of nitrobenzene removal percentage corresponds with the reactive trend among scavengers and sulfate radicals, whereas the rate constants between scavengers and hydroxyl radicals make an insignificant difference. It reveals that sulfate radicals were responsible for nitrobenzene oxidation in wastewater.

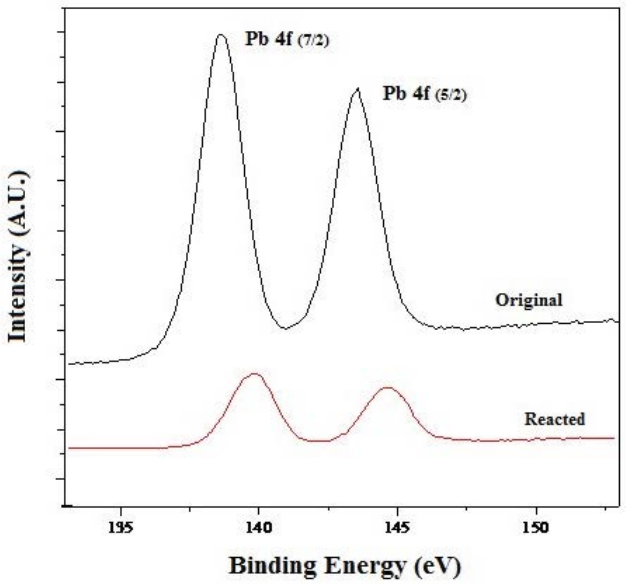

Fig. 5. X-ray photoelectron spectra of Pb 4f core level for original Ag(5 wt.%)/PbO and reacted Ag(5 wt.%)/PbO semiconductors.

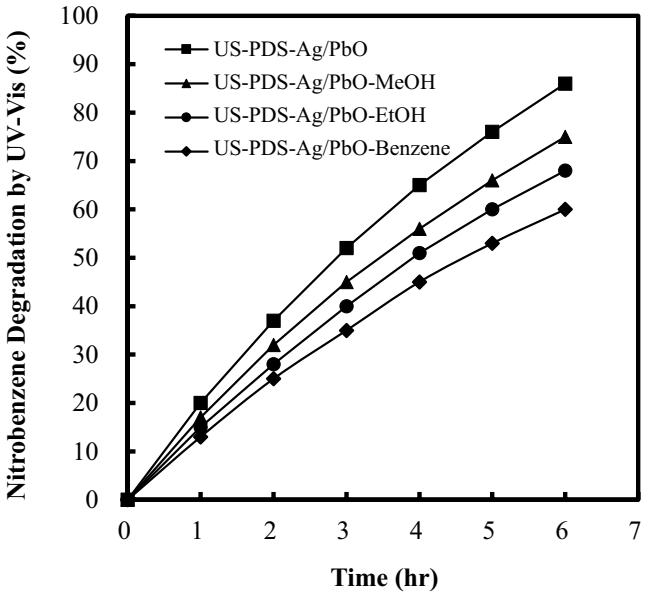

Fig. 6. Effect of coexistence of benzene, ethanol, and methanol, respectively, on the nitrobenzene degradation percentage under the conditions of ultrasonic power intensity = 240 W cm^{-2}, T = 318 K, persulfate concentration = 60 mM, and Ag(5 wt.%)/PbO dosage = 1.0 g L^{-1}.

3.4. Effect of ultrasonic power intensity on persulfate coupled with Ag/PbO under ultrasonic irradiation

As far as ultrasonic energy efficiency is concerned, the ultrasonic power intensity executed on persulfate coupled with Ag/PbO was varied. TOC removal percentages at the time-dependent format were shown in a variety of ultrasonic power intensity (Fig. 7a). It is evident that the

nitrobenzene decomposition rate increased with an increase of ultrasonic power intensity. The yield of sulfate radicals was expected on increasing, caused by more cavitation events. Conversely, the highest power intensity imposed (300 W cm^{-2}) was adverse to the nitrobenzene removal efficiency. The ultimate operating conditions would result in significant enhancement on the quantity of microbubbles, which intended to grow together into larger bubbles and diminished cavitation strength. Therefore, ultrasonic energy efficiency was reduced and gave rise to the formation of lesser amounts of sulfate radicals. This phenomenon was directly reflected in the trend of the scavenging index (Fig. 7b). An analogous declaration was pointed out by Sivakumar and Pandit et al. [65] and Sivakumar et al. [66], of which research evaluated the optimal ultrasonic power intensity. Furthermore, the ultrasound would bring about degassing effect in the aqueous phase [67]. The amount of hydroxyl radicals descended from oxygen and sono-generated electrons over Ag/PbO would reduce (refer to Eq. (5)) as a result of decrement in oxygen gas dissolved. Nonetheless, higher ultrasonic power intensity accelerated nitrobenzene removal rate. It means that sulfate radicals played an important role in oxidation of nitrobenzene:

$$O_2 + 2H_2O + 3e^-_{cb} \rightarrow 3OH^- + {}^{\bullet}OH \quad (5)$$

3.5. Effect of persulfate concentrations on persulfate coupled with Ag/PbO under ultrasonic irradiation

The optimal persulfate concentration applied is an important issue as regards economic consideration. As given in Fig. 8a, the TOC removal percentage at the time-dependent format was presented in a series of persulfate concentrations. It is apparent that the nitrobenzene removal rate increased upon increasing persulfate concentrations. Thanks to the existence of high persulfate concentrations, high yields of sulfate radicals were expected to be produced. In contrast, the decomposition rate of nitrobenzene was decreased at the excess persulfate concentration (80 mM). The observation may be ascribed to the occurrence of unexpected reactions between sulfate radicals and over-dosage of persulfate anions [47,68]. Moreover, nitrobenzene oxidation was carried out in the presence of benzene simultaneously to distinguish yields of sulfate radicals by the scavenging index (Fig. 8b). As expected, the scavenging index displays dramatically a similar tendency with both sulfate radical yields and TOC removal patterns. Thus, it advocates that sulfate radicals were the main oxidants.

3.6. Effect of Ag/PbO dosage on persulfate coupled with Ag/PbO under ultrasonic irradiation

An optimal dosage of Ag/PbO semiconductor needs to be established for promotion degradation efficiency of nitrobenzene. The dosage effect referred to sonocatalysis of Ag/PbO on persulfate activation is shown in Fig. 9a. Obviously, the TOC removal rate increased with increasing dosages of Ag/PbO, whereas it decreased under the over-dosage of Ag/PbO (≧1.6 g L^{-1}). The enhancement on the nitrobenzene oxidation rate may be attributed to stronger activation of persulfate anions by sonocatalysis of Ag/PbO (refer to Eq. (3)), leading to high yields of sulfate radicals. Nonetheless, acoustic waves would be retarded on account of the excess of Ag/PbO powder (≧1.6 g L^{-1}) [69,70]. TOC degradation rate exhibited an identical trend as the scavenging index (Fig. 9b). It implies that sulfate radicals were the

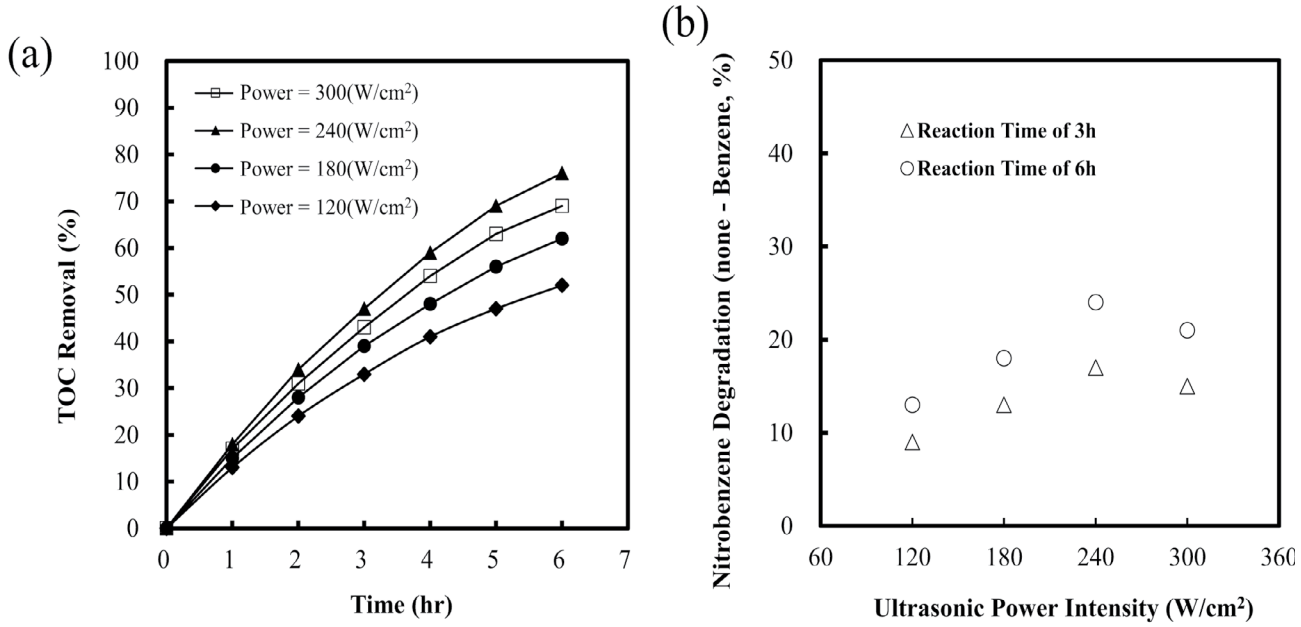

Fig. 7. (a) Effect of ultrasonic power intensity on the TOC removal percentage under the conditions of T = 318 K, persulfate concentration = 60 mM, and Ag(5 wt.%)/PbO dosage = 1.0 g L^{-1}. (b) Difference of nitrobenzene degradation percentage between the absence of benzene and presence of benzene under the conditions of T = 318 K, persulfate concentration = 60 mM, and Ag(5 wt.%)/PbO dosage = 1.0 g L^{-1}, detected by UV-vis and served as scavenging index.

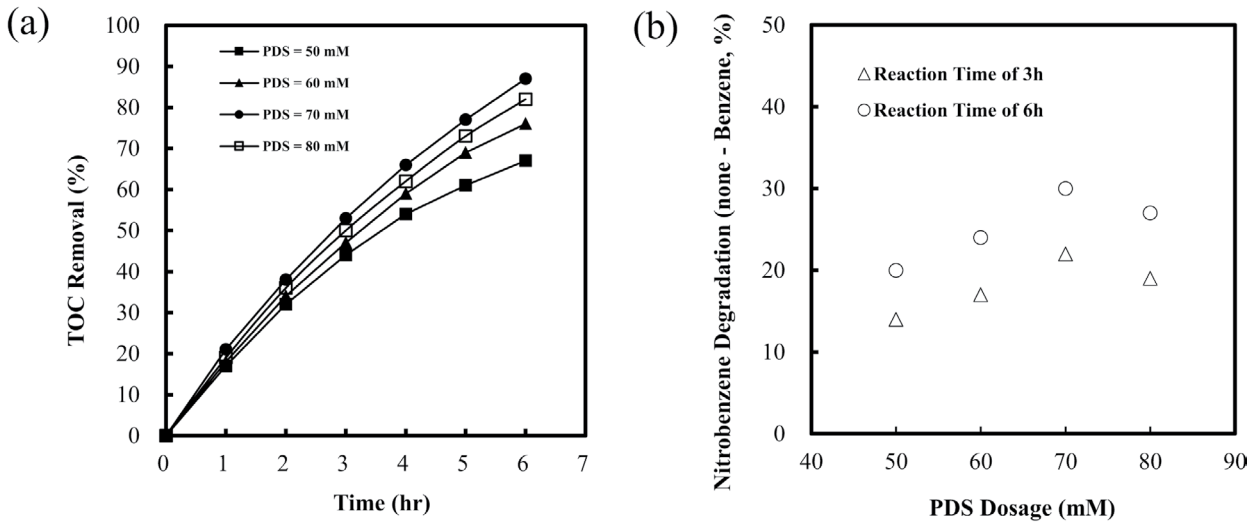

Fig. 8. (a) Effect of persulfate concentrations on the TOC removal percentage under the conditions of ultrasonic power intensity = 240 W cm^{-2}, T = 318 K, and Ag(5 wt.%)/PbO dosage = 1.0 g L^{-1}. (b) Difference of nitrobenzene degradation percentage between the absence of benzene and presence of benzene under the conditions of ultrasonic power intensity = 240 W cm^{-2}, T = 318 K and Ag(5 wt.%)/PbO dosage = 1.0 g L^{-1}, detected by UV-vis and served as scavenging index.

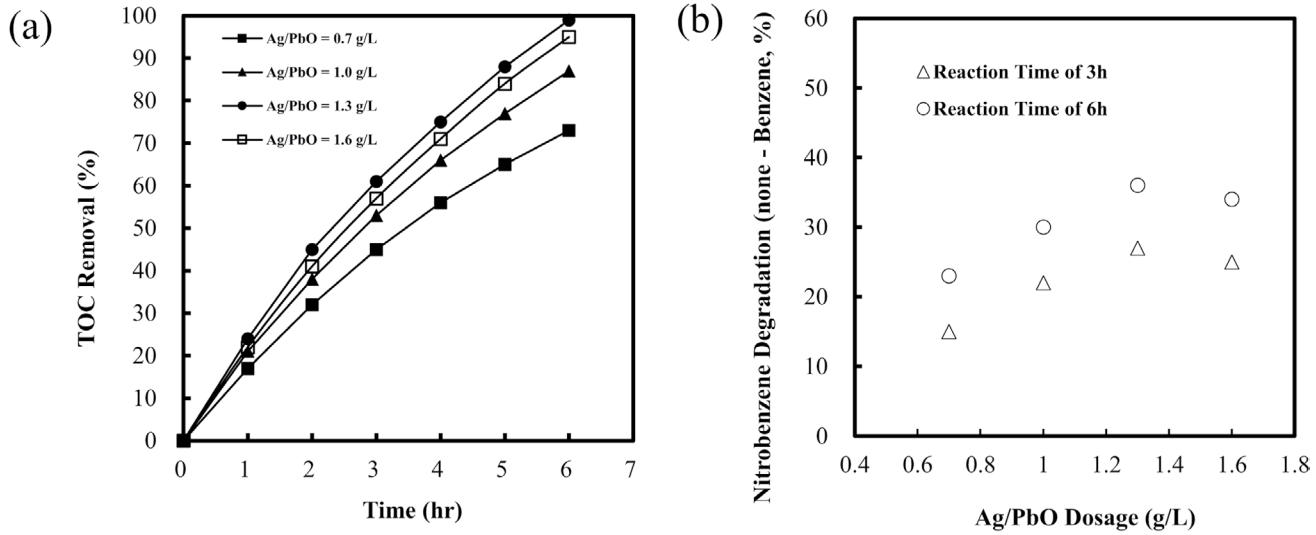

Fig. 9. (a) Effect of Ag(5 wt.%)/PbO dosages on the TOC removal percentage under the conditions of ultrasonic power intensity = 240 W cm^{-2}, T = 318 K, and persulfate concentration = 70 mM. (b) Difference of nitrobenzene degradation percentage between the absence of benzene and presence of benzene under the conditions of ultrasonic power intensity = 240 W cm^{-2}, T = 318 K, and persulfate concentration = 70 mM, detected by UV-vis and served as scavenging index.

main oxidizing agents toward the decomposition of nitrobenzene. Particularly, the optimal conditions for complete oxidation of nitrobenzene were found as follows: ultrasonic power intensity = 240 W cm^{-2}, T = 318 K, persulfate concentration = 70 mM and Ag/PbO dosage = 1.3 g L^{-1}.

3.7. Effect of initial pH values on persulfate coupled with Ag/PbO under ultrasonic irradiation

For the sake of enhancing the mineralization of nitrobenzene, the acidity of wastewater was usually changed. Fig. 10 illustrates the time-dependent format of TOC removal percentage under a series of initial pH values. Obviously, the nitrobenzene decomposition efficiency showed an insignificant difference among the pH values tested (3.0–7.0). The observation may be interpreted with the self-decomposition of persulfate anions partially into peroxymonosulfate (refer to Eq. (6)) [71]. The acidity of wastewater would drop nearly to the pH value of 2.0 upon the addition of persulfate anions for all initial pH values mentioned. Despite of difference in initial pH values, nitrobenzene oxidation was performed at approximate acidity

of pH 1.6 to 2.0, wherein sulfate radicals were recognized to be the main oxidants [46,72]. Thus, it supports that sulfate radicals were principal oxidizing agents:

$$S_2O_8^{2-} + H_2O \rightarrow H_2SO_5 + SO_4^{2-} \quad (6)$$

3.8. Reaction pathways of nitrobenzene by persulfate coupled with Ag/PbO under ultrasonic irradiation

All organic compounds extracted at the duration performed by persulfate cooperated with Ag/PbO under ultrasonic irradiation were analyzed using a GC-MS spectrometer. Table 3 summarizes the components acquired, including nitrobenzene feedstock, 2-nitrophenol, 4-nitrophenol, phenol, hydroquinone, and *p*-benzoquinone. For consideration of 2-nitrophenol and 4-nitrophenol, they seem to be derived from hydroxycyclohexadienyl radicals, which undergo O_2 addition and sequential $HO_2^{\bullet}$ elimination to form hydroxylated products [64,73]. It indicates explicitly the occurrence of nitrophenol denitration on account of detection of phenol [74]. Then, phenol was partially oxidized into hydroquinone, which would be successively converted into *p*-benzoquinone by way of hydrogen abstraction. The ultimate products for nitrobenzene oxidation consist of nitrate ions (sensed at UV-vis 313 nm), carbon dioxide, and water. In light of degradation intermediates authenticated, the possible pathways for nitrobenzene oxidation by persulfate integrated with Ag/PbO activated with ultrasound could be demonstrated in Fig. 11.

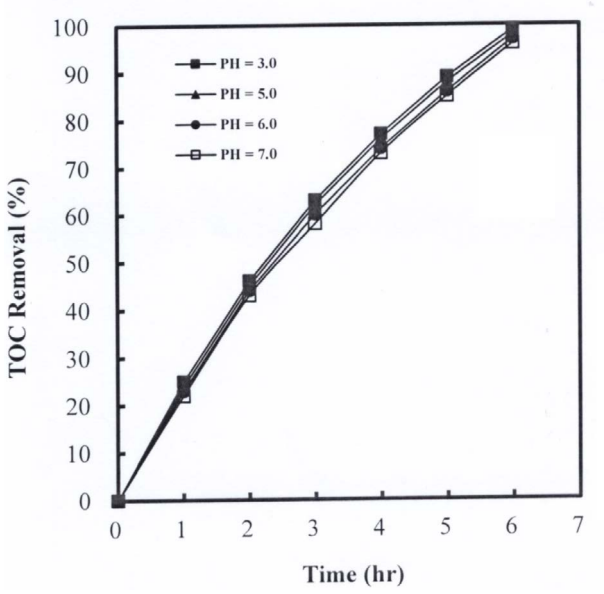

Fig. 10. Effect of initial pH values on the TOC removal percentage under the conditions of ultrasonic power intensity = 240 W cm^{-2}, T = 318 K, persulfate concentration = 70 mM and Ag(5 wt.%)/PbO dosage = 1.3 g L^{-1}.

4. Conclusions

According to the above discussion mentioned, nitrobenzene contaminants were predominantly mineralized by reactive sulfate radicals, descended from persulfate integrated with Ag/PbO semiconductors activated with ultrasound. It was supported by the scavenging experiments, wherein nitrobenzene removal rates were retarded sequentially with benzene, ethanol, and methanol. In accordance with GC-MS analyses, the plausible pathways for nitrobenzene oxidation are hypothesized as follows. Nitrobenzene was preliminarily transformed into hydroxycyclohexadienyl radicals, subsequent oxidation to 2-nitrophenol and 4-nitrophenol, independently. Nitrophenol species were evidently denitrated to phenol. Oxidation of phenol resulted in the sequential synthesis of hydroquinone and *p*-benzoquinone. In the end, nitrobenzene could be entirely mineralized into nitrate ions, carbon dioxide, and water. It deserves to note that nitrobenzene in wastewater was totally abated. The dramatic results persuade us that persulfate combined with Ag/PbO under ultrasonic irradiation may be a potential manner for wastewater disposal.

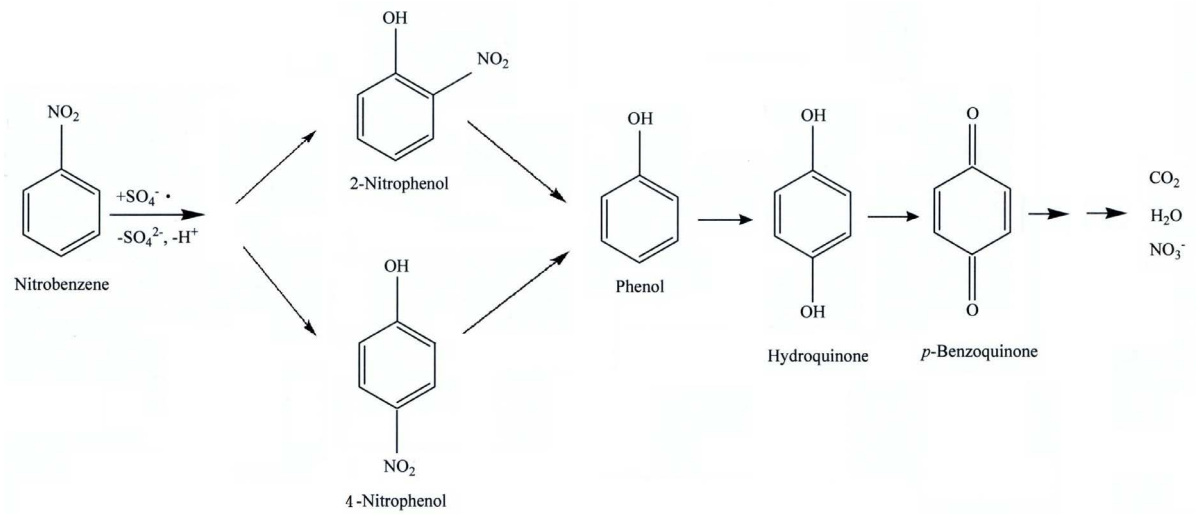

Fig. 11. Plausible degradation pathways of nitrobenzene in aqueous solution by persulfate coupled with Ag/PbO under ultrasonic irradiation.

Table 3
Compositions of feedstock and degradation intermediates identified by GC-MS

Component	m/z (relative abundance, %)
Feedstock	
Nitrobenzene	50 (15.3), 51 (37.5), 65 (13.2), 74 (8.5), 77 (100), 78 (6.9), 93 (16.6), 123 (69.7), 124 (5.5)
Degradation intermediate	
2-Nitrophenol	39 (15.3), 53 (9.2), 63 (19.7), 64 (13.5), 65 (25.0), 81 (19.3), 93 (7.7), 109 (17.7), 139 (100)
4-Nitrophenol	39 (43.9), 53 (22.8), 62 (13.6), 63 (27.7), 65 (79.5), 81 (32.5), 93 (26.6), 109 (66.7), 139 (100)
Phenol	38 (4.7), 39 (12.1), 40 (6.5), 55 (6.0), 63 (6.0), 65 (20.5), 66 (26.9), 94 (100), 95 (7.2)
Hydroquinone	39 (6.5), 53 (14.0), 54 (12.4), 55 (10.1), 81 (25.0), 82 (11.7), 110 (100), 111 (5.7), 143 (9.1)
p-Benzoquinone	26 (17.6), 52 (17.4), 53 (16.7), 54 (62.9), 80 (27.9), 82 (35.8), 108 (100), 109 (7.7), 110 (11.7)

References

[1] K. Weissermel, H.-J. Arpe, Ullmann's Encyclopedia of Industrial Chemistry, Vol. A17, 5th ed., VCH, Weinheim, 1991.
[2] G.X. Wang, X.Y. Zhang, C.Z. Yao, M.Z. Tian, Acute toxicity and mutagenesis of three metabolites mixture of nitrobenzene in mice, Toxicol. Ind. Health, 27 (2011) 167–171.
[3] J.W. Holder, Nitrobenzene carcinogenicity in animals and human hazard evaluation, Toxicol. Ind. Health, 15 (1999) 445–457.
[4] L. Zhu, B. Ma, L. Zhang, The study of distribution and fate of nitrobenzene in a water/sediment microcosm, Chemosphere, 69 (2007) 1579–1585.
[5] I. Nitoi, P. Oancea, M. Raileanu, M. Crisan, L. Constantin, I. Cristea, UV-VIS photocatalytic degradation of nitrobenzene from water using heavy metal doped titania, J. Ind. Eng. Chem., 21 (2015) 677–682.
[6] R.J. Tayade, H.C. Bajaj, R.V. Jasra, Photocatalytic removal of organic contaminants from water exploiting tuned band gap photocatalysts, Desalination, 275 (2011) 160–165.
[7] X.Z. Shen, Z.C. Liu, S.M. Xie, J. Guo, Degradation of nitrobenzene using titania photocatalysts co-doped with nitrogen and cerium under visible light illumination, J. Hazard. Mater., 162 (2009) 1193–1198.
[8] L. Zhao, W. Ma, J. Ma, G. Wen, Q. Liu, Relationship between acceleration of hydroxyl radical initiation and increase of multiple-ultrasonic field amount in the process of ultrasound catalytic ozonation for degradation of nitrobenzene in aqueous solution, Ultrason. Sonochem., 22 (2015) 198–204.
[9] L.K. Weavers, F.H. Ling, M.R. Hoffmann, Aromatic compound degradation in water using a combination of sonolysis and ozonolysis, Environ. Sci. Technol., 32 (1998) 2727–2733.
[10] L. Zhao, J. Ma, Z.Z. Sun, Oxidation products and pathway of ceramic honeycomb-catalyzed ozonation for the degradation of nitrobenzene in aqueous solution, Appl. Catal., B, 79 (2008) 244–253.
[11] L. Zhao, J. Ma, Z.Z. Sun, X.D. Zhai, Catalytic ozonation for the degradation of nitrobenzene in aqueous solution by ceramic honeycomb-supported manganese, Appl. Catal., B, 83 (2008) 256–264.
[12] L. Zhao, J. Ma, Z.Z. Sun, X.D. Zhai, Preliminary kinetic study on the degradation of nitrobenzene by modified ceramic honeycomb-catalytic ozonation in aqueous solution, J. Hazard. Mater., 161 (2009) 988–994.
[13] L. Zhao, J. Ma, Z.Z. Sun, H. Liu, Mechanism of heterogeneous catalytic ozonation of nitrobenzene in aqueous solution with modified ceramic honeycomb, Appl. Catal., B, 89 (2009) 326–334.
[14] L. Zhao, J. Ma, Z.Z. Sun, H. Liu, Influencing mechanism of temperature on the degradation of nitrobenzene in aqueous solution by ceramic honeycomb catalytic ozonation, J. Hazard. Mater., 167 (2009) 1119–1125.
[15] C. Chen, X. Yan, B.A. Yoza, T. Zhou, Y. Li, Y. Zhan, Q. Wang, Q.X. Li, Efficiencies and mechanisms of ZSM5 zeolites loaded with cerium, iron, or manganese oxides for catalytic ozonation of nitrobenzene in water, Sci. Total Environ., 612 (2018) 1424–1432.
[16] Y. Chen, H. Li, W. Liu, Y. Tu, Y. Zhang, W. Han, L. Wang, Electrochemical degradation of nitrobenzene by anodic oxidation on the constructed TiO_2-NTs/SnO_2-Sb/PbO_2 electrode, Chemosphere, 113 (2014) 48–55.
[17] K. Xia, F. Xie, Y. Ma, Degradation of nitrobenzene in aqueous solution by dual-pulse ultrasound enhanced electrochemical process, Ultrason. Sonochem., 21 (2014) 549–553.
[18] D. Gu, J. Dong, Y. Zhang, L. Zhu, C. Yan, H. Wu, B. Wang, An insight into pathways of solar-driven STEP oxidation of nitrobenzene by an integrated *in situ* thermoelectrochemical microreactor-analyzer, J. Cleaner Prod., 200 (2018) 1026–1033.
[19] B.C. Jiang, Z.Y. Lu, F.Q. Liu, A.M. Li, J.J. Dai, L. Xu, L.M. Chu, Inhibiting 1,3-dinitrobenzene formation in Fenton oxidation of nitrobenzene through a controllable reductive pretreatment with zero-valent iron, Chem. Eng. J., 174 (2011) 258–265.
[20] L. Carlos, D. Nichela, J.M. Triszcz, J.I. Felice, F.S.G. Einschlag, Nitration of nitrobenzene in Fenton's processes, Chemosphere, 80 (2010) 340–345.
[21] Y. Zhang, K. Zhang, C. Dai, X. Zhou, H. Si, An enhanced Fenton reaction catalyzed by natural heterogeneous pyrite for nitrobenzene degradation in an aqueous solution, Chem. Eng. J., 244 (2014) 438–445.
[22] D.A. Nichela, A.M. Berkovic, M.R. Costante, M.P. Juliarena, F.S.G. Einschlag, Nitrobenzene degradation in Fenton-like systems using Cu(II) as catalyst. Comparison between Cu(II)- and Fe(III)-based systems, Chem. Eng. J., 228 (2013) 1148–1157.
[23] D. Nichela, L. Carlos, F.S.G. Einschlag, Autocatalytic oxidation of nitrobenzene using hydrogen peroxide and Fe(III), Appl. Catal., B, 82 (2008) 11–18.
[24] Y. Sun, Z. Yang, P. Tian, Y. Sheng, J. Xu, Y.F. Han, Oxidative degradation of nitrobenzene by a Fenton-like reaction with Fe-Cu bimetallic catalysts, Appl. Catal., B, 244 (2019) 1–10.
[25] H. Duan, Y. Liu, X. Yin, J. Bai, J. Qi, Degradation of nitrobenzene by Fenton-like reaction in a H_2O_2/schwertmannite system, Chem. Eng. J., 283 (2016) 873–879.
[26] G.M.S. Elshafei, F.Z. Yehia, O.I.H. Dimitry, A.M. Badawi, G. Eshaq, Ultrasonic assisted-Fenton-like degradation of nitrobenzene at neutral pH using nanosized oxide of Fe and Cu, Ultrason. Sonochem., 21 (2014) 1358–1365.
[27] J. Anotai, P. Sakulkittimasak, N. Boonrattanakij, M.C. Lu, Kinetics of nitrobenzene oxidation and iron crystallization in fluidized-bed Fenton process, J. Hazard. Mater., 165 (2009) 874–880.
[28] C. Ratanatamskul, S. Chintitanun, N. Masomboon, M.C. Lu, Inhibitory effect of inorganic ions on nitrobenzene oxidation by fluidized-bed Fenton process, J. Mol. Catal. A: Chem., 331 (2010) 101–105.
[29] Y. Ji, Y. Shi, L. Wang, J. Lu, Denitration and renitration processes in sulfate radical-mediated degradation of nitrobenzene, Chem. Eng. J., 315 (2017) 591–597.

[30] A. De Luca, X. He, D.D. Dionysiou, R.F. Dantas, S. Esplugas, Effects of bromide on the degradation of organic contaminants with UV and Fe^{2+} activated persulfate, Chem. Eng. J., 318 (2017) 206–213.
[31] J. Qiao, S. Luo, P. Yang, W. Jiao, Y. Liu, Degradation of nitrobenzene-containing wastewater by ozone/persulfate oxidation process in a rotating packed bed, J. Taiwan Inst. Chem. Eng., 99 (2019) 1–8.
[32] J. Guo, L. Zhu, N. Sun, Y. Lan, Degradation of nitrobenzene by sodium persulfate activated with zero-valent zinc in the presence of low frequency ultrasound, J. Taiwan Inst. Chem. Eng., 78 (2017) 137–143.
[33] Y. Pan, M. Zhou, X. Li, L. Xu, Z. Tang, X. Sheng, B. Li, Highly efficient persulfate oxidation process activated with pre-magnetization Fe^0, Chem. Eng. J., 318 (2017) 50–56.
[34] Y. Zhang, X. Xu, Y. Pan, L. Xu, M. Zhou, Pre-magnetized Fe^0 activated persulphate for the degradation of nitrobenzene in groundwater, Sep. Purif. Technol., 212 (2019) 555–562.
[35] T.J. Matula, R.A. Roy, P.D. Mourad, W.B. McNamara Iii, K.S. Suslick, Comparison of multibubble and single-bubble sonoluminescence spectra, Phys. Rev. Lett., 75 (1995) 2602–2605.
[36] R.A. Hiller, S.J. Putterman, K.R. Weninger, Time-resolved spectra of sonoluminescence, Phys. Rev. Lett., 80 (1998) 1090–1093.
[37] W.S. Chen, Y.C. Shih, Mineralization of aniline in aqueous solution by sono-activated peroxydisulfate enhanced with PbO semiconductor, Chemosphere, 239 (2020) 124686 (1–9), doi: 10.1016/j.chemosphere.2019.124686.
[38] D. Pavlov, Semiconductor mechanism of the processes during electrochemical oxidation of PbO to PbO_2, J. Electroanal. Chem., 118 (1981) 167–185.
[39] I. Mukhopadhyay, S. Ghosh, M. Sharon, Surface modification by the potential delay technique to obtain a photoactive PbO film, Surf. Sci., 384 (1997) 234–239.
[40] M. Mohammadikish, K. Zamani, Controlled construction of uniform pompon-like Pb-ICP microarchitectures as a precursor for PbO semiconductor nanoflakes, Adv. Powder Technol., 29 (2018) 2813–2821.
[41] W.S. Chen, S.L. Huang, Photocatalytic degradation of bisphenol-A in aqueous solution by calcined PbO semiconductor irradiated with visible light, Desal. Water Treat., 190 (2020) 147–155.
[42] W.S. Chen, Y.C. Su, Removal of dinitrotoluenes in wastewater by sono-activated persulfate, Ultrason. Sonochem., 19 (2012) 921–927.
[43] S.L. He, L.P. Wang, J. Zhang, M.F. Hou, Fenton pre-treatment of wastewater containing nitrobenzene using ORP for indicating the endpoint of reaction, Procedia Earth planet. Sci., 1 (2009) 1268–1274.
[44] N.S. Satdeve, R.P. Ugwekar, B.A. Bhanvase, Ultrasound assisted preparation and characterization of Ag supported on ZnO nanoparticles for visible light degradation of methylene blue dye, J. Mol. Liq., 291 (2019) 111313 (1–11), doi: 10.1016/j.molliq.2019.111313.
[45] W.S. Chen, C.P. Huang, Mineralization of aniline in aqueous solution by electro-activated persulfate oxidation enhanced with ultrasound, Chem. Eng. J., 266 (2015) 279–288.
[46] C.J. Liang, H.W. Su, Identification of sulfate and hydroxyl radicals in thermally activated persulfate, Ind. Eng. Chem. Res., 48 (2009) 5558–5562.
[47] H. Lin, J. Wu, H. Zhang, Degradation of bisphenol A in aqueous solution by a novel electro/Fe^{3+}/peroxydisulfate process, Sep. Purif. Technol., 117 (2013) 18–23.
[48] K.P. Jyothi, S. Yesodharan, E.P. Yesodharan, Ultrasound (US), Ultraviolet light (UV) and combination (US + UV) assisted semiconductor catalyzed degradation of organic pollutants in water: oscillation in the concentration of hydrogen peroxide formed *in situ*, Ultrason. Sonochem., 21 (2014) 1787–1796.
[49] Y. Sakthivel, G. Venugopal, A. Durairaj, S. Vasanthkumar, X. Huang, Utilization of the internal electric field in semiconductor photocatalysis: a short review, J. Ind. Eng. Chem., 72 (2019) 18–30.
[50] X. Zhang, Y. Wang, F. Hou, H. Li, Y. Yang, X. Zhang, Y. Yang, Y. Wang, Effects of Ag loading on structural and photocatalytic properties of flower-like ZnO microspheres, Appl. Surf. Sci., 391 (2017) 476–483.
[51] Z. Han, L. Ren, Z. Cui, C. Chen, H. Pan, J. Chen, Ag/ZnO flower heterostructures as a visible-light driven photocatalyst via surface plasmon resonance, Appl. Catal., B, 126 (2012) 298–305.
[52] X. Li, W. Zhang, W. Cui, J. Li, Y. Sun, G. Jiang, H. Huang, Y. Zhang, F. Dong, Reactant activation and photocatalysis mechanisms on Bi-metal@Bi_2GeO_5 with oxygen vacancies: a combined experimental and theoretical investigation, Chem Eng. J., 370 (2019) 1366–1375.
[53] W. Cui, L. Chen, J. Li, Y. Zhou, Y. Sun, G. Jiang, S.C. Lee, F. Dong, Ba-vacancy induces semiconductor-like photocatalysis on insulator $BaSO_4$, Appl. Catal., B, 253 (2019) 293–299.
[54] S.K. Maji, N. Mukherjee, A.K. Dutta, D.N. Srivastava, P. Paul, B. Karmakar, A. Mondal, B. Adhikary, Deposition of nanocrystalline CuS thin film from a single precursor: structural, optical and electrical properties, Mater. Chem. Phys., 130 (2011) 392–397.
[55] V. Štengl, T.M. Grygar, The simplest way to Iodine-doped anatase for photocatalysts activated by visible light, Int. J. Photoenergy, 2011 (2011) 685935–685948.
[56] E. Kamaraj, S. Somasundaram, K. Balasubramani, M.P. Eswaran, R. Muthuramalingam, S. Park, Facile fabrication of CuO-Pb_2O_3 nanophotocatalysts for efficient degradation of Rose Bengal dye under visible light irradiation, Appl. Surf. Sci., 433 (2018) 206–212.
[57] L.M. Droessler, H.E. Assender, A.A.R. Watt, Thermally deposited lead oxides for thin film photovoltaics, Mater. Lett., 71 (2012) 51–53.
[58] Y.C. Lai, J.C. Lin, C. Lee, Nucleation and growth of highly oriented lead titanate thin films prepared by a sol-gel method, Appl. Surf. Sci., 125 (1998) 51–57.
[59] M. Salavati-Niasari, F. Mohandes, F. Davar, Preparation of PbO nanocrystals via decomposition of lead oxalate, Polyhedron, 28 (2009) 2263–2267.
[60] F.Y. Liu, J.H. Lin, Y.M. Dai, L.W. Chen, S.T. Huang, T.W. Yeh, J.L. Chang, C.C. Chen, Preparation of perovskites $PbBiO_2I$/PbO exhibiting visible-light photocatalytic activity, Catal. Today, 314 (2018) 28–41.
[61] C.H. Park, M.S. Won, Y.H. Oh, Y.G. Son, An XPS study and electrical properties of $Pb_{1.1}Zr_{0.53}Ti_{0.47}O_3$/PbO/Si (MFIS) structures according to the substrate temperature of the PbO buffer layer, Appl. Surf. Sci., 252 (2005) 1988–1997.
[62] D.A. Zatsepin, D.W. Boukhvalov, N.V. Gavrilov, A.F. Zatsepin, V.Y. Shur, A.A. Esin, S.S. Kim, E.Z. Kurmaev, Soft electronic structure modulation of surface (thin-film) and bulk (ceramics) morphologies of TiO_2-host by Pb-implantation: XPS-and-DFT characterization, Appl. Surf. Sci., 400 (2017) 110–117.
[63] A. Kanca, D. Uner, *In situ* and downstream sulfidation reactivity of PbO and ZnO during pyrolysis and hydrogenation of a high-sulfur lignite, Int. J. Hydrogen Energy, 44 (2019) 18827–18835.
[64] P. Neta, R.E. Huie, A.B. Ross, Rate constants for reactions of inorganic radicals in aqueous solution, J. Phys. Chem. Ref. Data, 17 (1988) 1027–1284.
[65] M. Sivakumar, A.B. Pandit, Ultrasound enhanced degradation of Rhodamine B: optimization with power density, Ultrason. Sonochem., 8 (2001) 233–240.
[66] M. Sivakumar, P.A. Tatake, A.B. Pandit, Kinetics of *p*-nitrophenol degradation: effect of reaction conditions and cavitational parameters for a multiple frequency system, Chem. Eng. J., 85 (2002) 327–338.
[67] W.S. Chen, C.P. Huang, Decomposition of nitrotoluenes in wastewater by sonoelectrochemical and sonoelectro-Fenton oxidation, Ultrason. Sonochem., 21 (2014) 840–845.
[68] L.W. Hou, H. Zhang, X.F. Xue, Ultrasound enhanced heterogeneous activation of peroxydisulfate by magnetite catalyst for the degradation of tetracycline in water, Sep. Purif. Technol., 84 (2012) 147–152.
[69] C. Berberidou, I. Poulios, N.P. Xekoukoulotakis, D. Mantzavinos, Sonolytic, photocatalytic and sonophotocatalytic degradation of malachite green in aqueous solutions, Appl. Catal. B., 74 (2007) 63–72.

[70] W.S. Chen, S.C. Huang, Sonophotocatalytic degradation of dinitrotoluenes and trinitrotoluene in industrial wastewater, Chem. Eng. J., 172 (2011) 944–951.
[71] D.A. House, Kinetics and mechanism of oxidation by peroxydisulfate, Chem. Rev., 62 (1962) 185–203.
[72] E. Hayon, A. Treinin, J. Wilf, Electronic spectra, photochemistry, and autoxidation mechanism of the sulfite-bisulfite-pyrosulfite systems. The $SO_2^{-\bullet}$, $SO_3^{-\bullet}$, $SO_4^{-\bullet}$, and $SO_5^{\bullet}$ radicals, J. Am. Chem. Soc., 94 (1972) 47–57.
[73] G.P. Anipsitakis, D.D. Dionysiou, M.A. Gonzalez, Cobalt-mediated activation of peroxymonosulfate and sulfate radical attack on phenolic compounds. Implications of chlorine ions, Environ. Sci. Technol., 40 (2006) 1000–1007.
[74] J. Zhou, J. Xiao, D. Xiao, Y. Guo, C. Fang, X. Lou, Z. Wang, J. Liu, Transformations of chloro and nitro groups during the peroxymonosulfate-based oxidation of 4-chloro-2-nitrophenol, Chem. Eng. J., 134 (2015) 446–451.